Mixed Dimensionality of Confined Conducting Electrons in the Surface Region of $SrTiO_3$

N. C. Plumb,[1,*] M. Salluzzo,[2] E. Razzoli,[1] M. Månsson,[3,4,5] M. Falub,[1] J. Krempasky,[1] C. E. Matt,[1,5] J. Chang,[1,4] M. Schulte,[6] J. Braun,[6] H. Ebert,[6] J. Minár,[6,7] B. Delley,[8] K.-J. Zhou,[1,†] T. Schmitt,[1] M. Shi,[1] J. Mesot,[1,4,5] L. Patthey,[1,9] and M. Radović[1,4,9,‡]

[1]*Swiss Light Source, Paul Scherrer Institut, CH-5232 Villigen PSI, Switzerland*
[2]*CNR-SPIN, Complesso Universitario Monte S. Angelo, Via Cinthia I-80126, Napoli, Italy*
[3]*Laboratory for Neutron Scattering and Imaging, Paul Scherrer Institut, CH-5232 Villigen PSI, Switzerland*
[4]*Institute of Condensed Matter Physics, École Polytechnique Fédérale de Lausanne (EPFL), CH-1015 Lausanne, Switzerland*
[5]*Laboratory for Solid State Physics, ETH Zürich, CH-8093 Zürich, Switzerland*
[6]*Department Chemie, Ludwig-Maximilians-Universität München, 81377 München, Germany*
[7]*New Technologies—Research Center, University of West Bohemia, Univerzitni 8, 306 14 Pilsen, Czech Republic*
[8]*Condensed Matter Theory Group, Paul Scherrer Institut, CH-5232 Villigen PSI, Switzerland*
[9]*SwissFEL, Paul Scherrer Institut, CH-5232 Villigen PSI, Switzerland*

(Received 2 February 2014; published 18 August 2014)

Using angle-resolved photoemission spectroscopy, we show that the recently discovered surface state on $SrTiO_3$ consists of nondegenerate t_{2g} states with different dimensional characters. While the d_{xy} bands have quasi-2D dispersions with weak k_z dependence, the lifted d_{xz}/d_{yz} bands show 3D dispersions that differ significantly from bulk expectations and signal that electrons associated with those orbitals permeate the near-surface region. Like their more 2D counterparts, the size and character of the d_{xz}/d_{yz} Fermi surface components are essentially the same for different sample preparations. Irradiating $SrTiO_3$ in ultrahigh vacuum is one method observed so far to induce the "universal" surface metallic state. We reveal that during this process, changes in the oxygen valence band spectral weight that coincide with the emergence of surface conductivity are disproportionate to any change in the total intensity of the O 1*s* core level spectrum. This signifies that the formation of the metallic surface goes beyond a straightforward chemical doping scenario and occurs in conjunction with profound changes in the initial states and/or spatial distribution of near-E_F electrons in the surface region.

DOI: 10.1103/PhysRevLett.113.086801 PACS numbers: 73.20.-r, 79.60.-i

$SrTiO_3$ (STO) is a foundational material for the coming age of multifunctional oxide devices. Perhaps most famously, it hosts quasi-2D conducting states at interfaces with various transition metal oxides [1–5]. Moreover, it was recently shown that a low-dimensional metal can form on the bare surface of STO [6–8]. The discovery promises to extend this material's technological importance, as well as shed new light on the physics of metallic oxide surfaces and interfaces in general, so long as the properties and origin of the state can be understood and harnessed.

Although stoichiometric bulk STO is an insulator with a 3.2-eV band gap, photoemission experiments have observed metallicity in or on STO for many years [9,10]. However, the electronic structure and low-dimensional nature of the metallicity had not been deeply appreciated until very recent angle-resolved photoemission spectroscopy (ARPES) and scanning tunneling spectroscopy (STS) studies [6–8]. The ARPES measurements have revealed a highly 2D subband structure whose circular Fermi surface (FS) components and polarization selection rules indicate d_{xy} symmetry. However, depending on the measurement conditions, the spectra have occasionally glimpsed shallow bands consistent with $3d_{xz}/3d_{yz}$ states coexisting with the $3d_{xy}$ subbands [6,11]. The observations of these additional bands allude to a more complex FS topology than that of the d_{xy} subbands alone, but the properties of the shallow bands and their relationship to the surface state has so far not been deeply studied. Additionally, there are still open questions about the origin of the surface metallicity and the spectroscopic signatures associated with its formation.

To investigate these issues, we performed ARPES and core level x-ray photoemission spectroscopy (XPS) to study STO(001) wafers that were initially prepared to be highly TiO_2 terminated [12]. Just prior to the photoemission measurements, each sample was annealed *in situ* at 550 °C in 100 mbar of O_2 for about 2 h in order to establish a nominally oxygen-filled starting point. Certain samples then underwent subsequent *in situ* UHV annealing procedures in order to generate oxygen vacancies or other defects, thereby changing the nominal doping of each sample. In addition, one sample was lightly Nb doped (0.25% by weight, Nb-STO). More details of the sample treatments can be found in the Supplemental Material [12]. The resulting surfaces were studied without cleaving.

The ARPES measurements reveal four FS components, which are highlighted in Fig. 1. The data shown come from

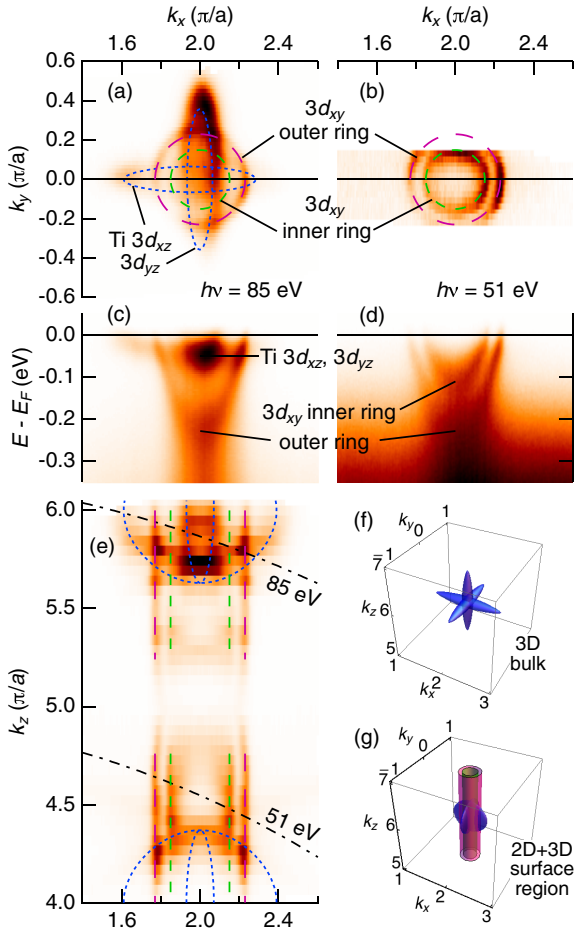

FIG. 1 (color online). Three-dimensional view of the near-E_F electronic structure of the metallic surface region on STO. (a) Fermi surface map in the k_x-k_y plane measured at $h\nu = 85$ eV. The data are from the Brillouin zone centered at $(k_x, k_y) = (2\pi/a, 0)$. The ellipsoidal Ti $3d_{xz}$ and $3d_{yz}$ bands are illustrated by dotted blue lines, while the Ti $3d_{xy}$ inner and outer rings are highlighted by short-dashed green lines and long-dashed magenta lines, respectively. (b) Analogous data taken at $h\nu = 51$ eV. (c),(d) Band dispersions along k_x at $k_y = 0$ for each of the above panels. (e) Fermi surface cut in the k_x-k_y plane at $k_y = 0$. The dot-dashed lines indicate the curvature of FS cuts in (a) and (b). (f) Expected shape of the 3D Fermi surface in the bulk. For reference, the FS volume shown here corresponds to a carrier density of about 4×10^{20} cm^{-3}. (g) Simplified representation of the mixed quasi-2D and 3D Fermi surface sheets at the STO surface. The colors correspond with the lines in (a)–(b).

Nb-STO, but all the samples are virtually identical in terms of the electronic structure at the surface. When measured using a photon energy of $h\nu = 85$ eV, the FS in the surface k_x-k_y plane is made up of two concentric rings (the inner of which has only very weak intensity), as well as two ellipsoids aligned along the k_x and k_y directions [Fig. 1(a)]. At other photon energies, the ellipsoids vanish while the rings remain, as demonstrated at $h\nu = 51$ eV [Fig. 1(b)]. Figures 1(c) and 1(d) show the corresponding dispersion cuts along $(k_x, k_y = 0)$ for (a) and (b), respectively. Based on their k_x-k_y symmetry, the ellipsoids can be associated with Ti $3d_{xz}/3d_{yz}$ orbitals and the rings with Ti $3d_{xy}$ orbitals. The inner ring has been proposed to be a quantum well subband of the outer ring [6,7] (i.e., the $n = 2$ quantum well state, while the outer ring is $n = 1$), but new experiments suggest the pair is instead related to Rashba-like spin-orbit coupling [20]. The rings had already been considered within the context of the surface metallic state [6,7]. Until now, however, the ellipsoids had never been fully characterized, and there were conflicting assessments of their dimensionalities and possible relation to the surface [6,11].

In ARPES, the different photon energies used to probe the FS in the k_x-k_y plane correspond to different planes cutting across the k_z axis [21]. Thus, by varying the photon energy, we mapped the complete FS of the metallic state on STO in three dimensions. Figure 1(e) shows the structure of the FS evaluated as a function of $\boldsymbol{k} = (k_x, 0, k_z)$. The outer ring has highly 2D character, though with a slight deviation in the Fermi momentum k_F near the Brillouin zone boundary at $k_z = 5\,\pi/a$. The inner ring is fairly cylindrical with long parallel segments, but near the zone boundaries along k_z it appears too close to form "end caps" of a pill-shaped FS component. These end caps likely signal a slight departure from a perfect 2D state, as similarly suggested by the warping of the outer ring near the zone boundary. We hence regard the inner and outer ring d_{xy} states as quasi-2D. Otherwise, the end caps may result from complicating factors such as matrix element effects or scattered weight due to an out-of-plane reconstruction, although so far we do not find clear evidence to support these scenarios.

Most interestingly, the d_{xz} and d_{yz} bands, which in bulk calculations [10,11] are expected to be prolate spheroids ["cigars," Fig. 1(f)], are actually stretched along the k_z axis ["flying saucers," Fig. 1(g)]. As a result, while in the k_x-k_y plane all carriers have effective masses in line with bulk expectations [10], the strong elongation of the d_{xz}/d_{yz} bands in k_z corresponds to a high effective mass in the out-of-plane direction ($m_z^* \approx 15 m_e$). (See Supplemental Material for more details about the extracted effective masses [12].) However, the d_{xz}/d_{yz} states, while distinct from truly bulklike electrons due to their substantially different z-axis dispersions, nevertheless show 3D character by virtue of their fully closed FS components along all $\boldsymbol{k}$ directions. We thus conclude that the d_{xz} and d_{yz} electrons penetrate multiple unit cells toward the bulk, while the d_{xy} electrons are more tightly confined to the surface. The overall picture is similar to the predicted orbital-resolved distribution of carriers in STO near the $LaAlO_3/STO(001)$ interface [22,23]. The measurements are in good qualitative and quantitative agreement with previous observations from variously annealed cleaved samples studied by ARPES using only select photon energies [6,7]. Thus the results here tie prior findings together and account for the visibility or invisibility of the ellipsoids in previous ARPES spectra of the metallic

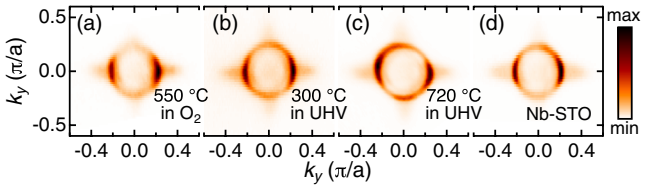

FIG. 2 (color online). Universality of the FS with respect to annealing conditions and light bulk doping. (a)–(d) Fermi surfaces of various STO samples (annealed in O_2 at 550 °C, annealed in UHV at 300 °C, annealed in UHV at 720 °C, and lightly Nb doped, respectively). The measurements were performed in the first Brillouin zone using $h\nu = 85$ eV, corresponding to roughly $k_z = 6.2\pi/a$, thus intersecting with the d_{xz}/d_{yz} ellipsoids.

surface, which can be attributed to the dimensionality of these states and the choice of measurement conditions (specifically the photon energy and Brillouin zone) that affect the momentum space being probed.

Like the quasi-2D rings [6], the sizes of the ellipsoids are essentially universal with respect to bulk oxygen vacancies or dopants (e.g., regardless of whether the samples are transparent or black), further confirming that these FS components are associated with the near-surface region, despite their 3D nature. This is illustrated in Figs. 2(a)–2(d), which show FSs measured on STO samples prepared by various *in situ* annealing treatments, as well as bulk Nb-doped STO.

So far it appears there may be multiple methods for preparing the metallic surface state on STO [6,8], including exposing the material to synchrotron radiation under UHV conditions ($\sim 10^{-11}$ mbar) typical for ARPES [7]. In Fig. 3(a), starting from an insulating, oxygen-annealed sample [the same as in Fig. 2(a)] that initially shows no FS, we expose a previously unstudied spot on the sample to the beam for an initial time t_0 (~10 min using $h\nu = 47$ eV) to establish the onset of surface metallicity. Sample charging is alleviated by a grounding technique described in the Supplemental Material [12]. During the beam exposure, the spectral weight associated with the O $2p$ valence band steadily decreases while a new feature grows inside the band gap of the bulk insulating STO. After 1 h, at t_f, the intensity of the valence band is about half the initial value at t_0 ($I_f/I_0 \sim 0.5$). This change coincides with the emergence and intensification of the signal at E_F, which appears to be (meta)stable for hours under UHV conditions, even when no beam is being applied (also noted in [7]).

Observations similar to Fig. 3(a) prompted speculation that photons generate oxygen vacancies that dope the surface [7]. Indeed, within the results obtained by us so far, photoinduced oxygen vacancies and/or other defects remain as plausible hypotheses to explain the origin of the carriers. However, by driving the decrease of the valence band intensity much further than in previous STO studies, the measurements here lead to new questions about the interpretation of this particular behavior. For example, the

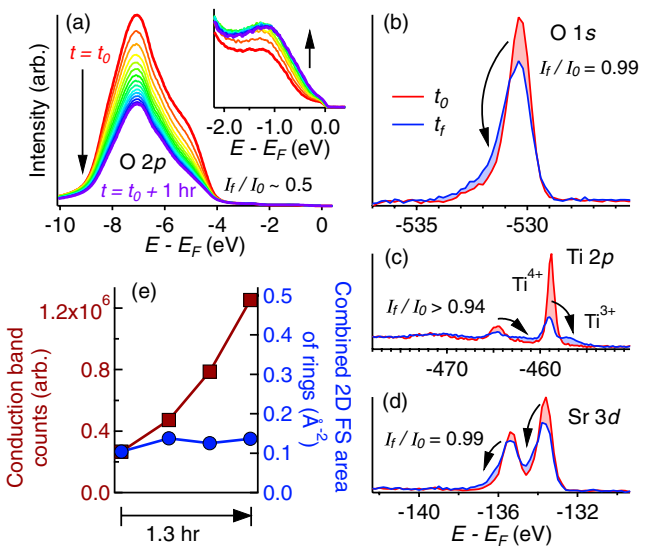

FIG. 3 (color online). Spectral evolution of the sample in Fig. 2(a) as a function of irradiation time. (a) Decrease of the O $2p$ valence band spectral intensity during irradiation. The inset highlights in-gap and metallic states that form during the same period. (b) XPS spectra of the O $1s$ core level measured before (t_0) and after (t_f) a similar radiation dose as in (a). (c), (d) Analogous spectra for the Ti $2p$ and Sr $3d$ core levels. (e) Comparison of the time evolution of total integrated counts in the conduction band region and the combined k-space areas of the inner and outer $3d_{xy}$ ring-shaped FS components.

universal FS in Figs. 1 and 2 corresponds to doping of only the t_{2g} states on the order of 0.1 e^- per unit cell, whereas, in principle, 50% oxygen-vacant STO (nominally 3 e^- per unit cell for $SrTiO_{1.5}$) would be expected to have completely occupied t_{2g} bands and an FS composed of e_g bands with 1 e^- per unit cell. Consequently, supposing that the O $2p$ intensity loss were purely due to oxygen depletion from the surface of STO, one should conclude that something like 90% of the electrons localize. Alternatively, we can consider that some other phenomenon (perhaps in addition to a limited amount of oxygen loss) significantly contributes to the decrease in valence band spectral weight.

To address this issue, Fig. 3(b) shows the XPS of the O $1s$ core level as a function of irradiation time. The spectra were taken at nominal t_0 (established at a newly exposed spot) and later, at t_f, after a dose of 47-eV photons approximately equivalent to the 1 h of irradiation in Fig. 3(a). The photon energy ($h\nu = 580$ eV for all core levels) was chosen to closely match the kinetic energies of the O $1s$ photoelectrons to those of the valence band states studied with $h\nu = 47$ eV. As a result, for the O $2p$ and O $1s$ peaks in Figs. 3(a) and 3(b), respectively, the photoelectron escape depths are equal, and thus the probing regions of the two techniques are identical. As the irradiation proceeds, the O $1s$ spectrum becomes asymmetrically distorted by transferring weight to the high binding energy sides of the peak. However, despite the change in the line shape, the

total O 1s signal intensity remains largely stable under photon irradiation. Integrating over the whole peak, the total count rate intensity of O 1s at t_0 and t_f is conserved to within about 1%, in stark contrast to the behavior of the oxygen valence band in Fig. 3(a). The Ti 2p and Sr 3d core levels, shown in Figs. 3(c) and 3(d), also undergo changes in their line shapes, with the Ti 2p peaks in particular showing a significant redistribution (~50%) from Ti^{4+} to Ti^{3+} states. Like O 1s, however, the energy-integrated intensities of these core levels are conserved to within a few percent. Various effects could account for the line shape changes. For instance, asymmetric skewing of the O 1s and Sr 3d peaks toward deeper binding energy may be related to photohole screening in the metallic state [24] and/or certain chemical changes, such as the possible formation of surface SrO [12,25].

The different behaviors of the valence band and core level signals as a result of irradiation should be understood in terms of the fundamentally different states being probed. Core level electrons are localized with well-defined orbital characters. By contrast, the orbital characters of valence states (and hence their photoemission matrix elements [21]) may change, and/or such electrons may spatially redistribute in the surface region, thus altering their visibility in photoemission—even absent a change in the surface composition [12]. Hence, the disproportionality between the changes in the valence band and XPS intensities under irradiation is a signature of non-negligible orbital or spatial changes of the near-E_F states during the formation of the surface metal.

Finally, we note that during the beam exposure, the FS quickly saturates to a relatively steady volume, while the signal intensity at the Fermi level continues to grow. This is demonstrated in Fig. 3(e), which compares total counts near the Fermi level (integrated within a single E vs k_x slice through $k_y = 0$ from −200 meV up to E_F) on the left axis with the total FS volume of the d_{xy} rings on the right axis as a function of time. The result indicates that impinging photons do not significantly influence the carrier concentration beyond a certain limit; they merely activate an increasingly large area of the sample surface to become metallic at a uniformly fixed carrier density, thus brightening the signal seen at the Fermi level. Moreover, as the signal intensifies, the ARPES features appear to sharpen while remaining 1×1 ordered in plane, thus suggesting that severe surface degradation does not occur [12]. This behavior, considered alongside the universality of the fully formed surface state with respect to various sample preparations (Fig. 2), self-consistently indicates that STO's surface transitions between two stable configurations—one nonmetallic and the other having a fixed density of free carriers with universal dispersions and distinct dimensionalities.

Despite clarifying the electronic structure of STO's surface, important questions surround the origin of the carriers and the microscopic process leading to the formation of the metallic state. For instance, various defects such as O vacancies or excess Sr might dope the surface, and even small amounts of defects allowed within the XPS presented so far (i.e., the roughly 1% reduction in O 1s intensity) could be sufficient to explain the observed FS volume. However, it is surprising to find the same electronic structure and surface carrier density over such a broad range of sample preparations. This includes samples annealed *in situ* starting from predominantly TiO_2-terminated wafers as in Figs. 2(a)–2(d), as well as cleaved surfaces of various annealed samples [6] where the nature and concentration of defects are likely to be significantly different [26]. Furthermore, as discussed, irradiating STO has a profound effect on the electrons' initial states that goes beyond merely doping the system in a rigid band manner. It is natural to think this corresponds with a widespread structural change in the surface region that is triggered directly by photons [27,28] and/or indirectly by relatively dilute photoinduced defects. Along these lines, one can propose that some common structural element of the surface conducting state (e.g., intralayer polar buckling as found in STO-based interface metallic systems [29–31] and even bare STO surfaces [32–34]) may be an important link between the variously treated samples that helps to explain the universality of their surfaces' electronic properties, despite nominally different compositions. Thus, obtaining a full understanding of the origins of the photoinduced spectral changes and their relation to the surface metallic state is a pressing matter that should prompt further investigations.

In conclusion, we have shown that the metallic state in the surface region of $SrTiO_3$ is composed of two kinds of confined carriers occupying quasi-2D d_{xy} and energetically lifted nonbulklike 3D d_{xz}/d_{yz} bands. Moreover, we find evidence that a process of generating metallicity at the surface of STO by photon irradiation involves a substantial change in the initial states of the valence electrons. Once formed, the metallic surface band structure and carrier density of both types of electrons are essentially universal with respect to diverse preparations of the samples. Similar electronic structure is likely to be relevant in confined surface or interface conducting states of related oxide systems. One example is $KTaO_3$ [35,36], whose metallic surface bands qualitatively resemble STO. There are also similarities to conducting STO-based interfaces, where there is evidence for two types of carriers and splitting of the d_{xy} and d_{xz}/d_{yz} states [31,37,38]. Furthermore, in $LaAlO_3$/STO it is predicted that the d_{xy} and d_{xz}/d_{yz} states should spatially segregate along the z axis in a manner qualitatively consistent with the dimensionalities of the respective FS components seen here on bare STO [22,23]. Thus, these new details of the electronic structure of STO's surface state should be valuable for understanding, creating, and manipulating functional oxide surfaces and interfaces.

Experiments were conducted at the Surface/Interface Spectroscopy (SIS) beam line of the Swiss Light Source within the Paul Scherrer Institut in Villigen, Switzerland. We are grateful for valuable conversations with J. H. Dil, V. N. Strocov, M. Kobayashi, C. Quitmann, A. Uldry, A. F. Santander-Syro, F. Fortuna, E. Rotenberg, R. Claessen, and F. Miletto Granozio. M. M. was partly supported by the Swedish Foundation BLANCEFLOR Boncompagni-Ludovisi née Bildt. M. F. acknowledges financial support from the Swiss National Science Foundation (Project-No. PMPDP2_128995). J. B., H. E., and J. Minár acknowledge financial support from the Deutsche Forschungsgemeinschaft (FOR 1346), the Bundesministerium für Bildung und Forschung (05K13WMA), and CENTEM (CZ.1.05/2.1.00/03.0088). C. M. was partially supported by the Swiss National Science Foundation and its NCCR MaNEP.

*nicholas.plumb@psi.ch
†Present address: Diamond Light Source, Harwell Science and Innovation Campus, Didcot, Oxon, OX11 0DE, United Kingdom.
‡milan.radovic@psi.ch

[1] A. Ohtomo and H. Y. Hwang, Nature (London) **427**, 423 (2004).
[2] Y. Hotta, T. Susaki, and H. Y. Hwang, Phys. Rev. Lett. **99**, 236805 (2007).
[3] P. Perna *et al.*, Appl. Phys. Lett. **97**, 152111 (2010).
[4] Y. Chen, N. Pryds, J. E. Kleibeuker, G. Koster, J. Sun, E. Stamate, B. Shen, G. Rijnders, and S. Linderoth, Nano Lett. **11**, 3774 (2011).
[5] Y. Z. Chen *et al.*, Nat. Commun. **4**, 1371 (2013).
[6] A. F. Santander-Syro *et al.*, Nature (London) **469**, 189 (2011).
[7] W. Meevasana, P. D. C. King, R. H. He, S.-K. Mo, M. Hashimoto, A. Tamai, P. Songsiriritthigul, F. Baumberger, and Z.-X. Shen, Nat. Mater. **10**, 114 (2011).
[8] R. Di Capua, M. Radovic, G. M. De Luca, I. Maggio-Aprile, F. Miletto Granozio, N. C. Plumb, Z. Ristic, U. Scotti di Uccio, R. Vaglio, and M. Salluzzo, Phys. Rev. B **86**, 155425 (2012).
[9] R. Courths, B. Cord, and H. Saalfeld, Solid State Commun. **70**, 1047 (1989).
[10] Y. Aiura, I. Hase, H. Bando, T. Yasue, T. Saitoh, and D. S. Dessau, Surf. Sci. **515**, 61 (2002).
[11] W. Meevasana *et al.*, New J. Phys. **12**, 023004 (2010).
[12] See Supplemental Material at http://link.aps.org/supplemental/10.1103/PhysRevLett.113.086801, which includes Refs. [13–19], and contains further details about the samples, preparation techniques, measurements, data analysis, and interpretation.
[13] G. Koster, B. L. Kropman, G. J. H. M. Rijnders, D. H. A. Blank, and H. Rogalla, Appl. Phys. Lett. **73**, 2920 (1998).
[14] T. Ohnishi, K. Shibuya, M. Lippmaa, D. Kobayashi, H. Kumigashira, M. Oshima, and H. Koinuma, Appl. Phys. Lett. **85**, 272 (2004).
[15] T. Nishimura, A. Ikeda, H. Namba, T. Morishita, and Y. Kido, Surf. Sci. **421**, 273 (1999).
[16] S. Singh, T.-Y. Chien, J. R. Guest, and M. R. Fitzsimmons, Phys. Rev. B **85**, 115450 (2012).
[17] Z. S. Popović, S. Satpathy, and R. M. Martin, Phys. Rev. Lett. **101**, 256801 (2008).
[18] D. A. Shirley, Phys. Rev. B **5**, 4709 (1972).
[19] M. P. Seah and W. A. Dench, Surf. Interface Anal. **1**, 2 (1979).
[20] A. F. Santander-Syro, F. Fortuna, C. Bareille, T. C. Rödel, G. Landolt, N. C. Plumb, J. H. Dil, and M. Radović (unpublished).
[21] A. Damascelli, Phys. Scr. **T109**, 61 (2004).
[22] P. Delugas, A. Filippetti, V. Fiorentini, D. I. Bilc, D. Fontaine, and P. Ghosez, Phys. Rev. Lett. **106**, 166807 (2011).
[23] Z. Zhong, Q. Zhang, and K. Held, Phys. Rev. B **88**, 125401 (2013).
[24] S. Doniach and M. Šunjić, J. Phys. C **3**, 285 (1970).
[25] S. Chambers, T. Droubay, C. Capan, and G. Sun, Surf. Sci. **606**, 554 (2012).
[26] N. P. Guisinger, T. S. Santos, J. R. Guest, T.-Y. Chien, A. Bhattacharya, J. W. Freeland, and M. Bode, ACS Nano **3**, 4132 (2009).
[27] S. Nozawa, T. Iwazumi, and H. Osawa, Phys. Rev. B **72**, 121101 (2005).
[28] Y. Qiu, C. Q. Wu, and K. Nasu, Phys. Rev. B **72**, 224105 (2005).
[29] S. A. Pauli, S. J. Leake, B. Delley, M. Björck, C. W. Schneider, C. M. Schlepütz, D. Martoccia, S. Paetel, J. Mannhart, and P. R. Willmott, Phys. Rev. Lett. **106**, 036101 (2011).
[30] C. Cantoni *et al.*, Adv. Mater. **24**, 3952 (2012).
[31] M. Salluzzo, S. Gariglio, X. Torrelles, Z. Ristic, R. Di Capua, J. Drnec, M. M. Sala, G. Ghiringhelli, R. Felici, and N. B. Brookes, Adv. Mater. **25**, 2333 (2013).
[32] N. Bickel, G. Schmidt, K. Heinz, and K. Müller, Phys. Rev. Lett. **62**, 2009 (1989).
[33] T. Hikita, T. Hanada, M. Kudo, and M. Kawai, Surf. Sci. **287–288**, 377 (1993).
[34] A. Ikeda, T. Nishimura, T. Morishita, and Y. Kido, Surf. Sci. **433–435**, 520 (1999).
[35] P. D. C. King *et al.*, Phys. Rev. Lett. **108**, 117602 (2012).
[36] A. F. Santander-Syro *et al.*, Phys. Rev. B **86**, 121107 (2012).
[37] K.-J. Zhou, M. Radovic, J. Schlappa, V. Strocov, R. Frison, J. Mesot, L. Patthey, and T. Schmitt, Phys. Rev. B **83**, 201402(R) (2011).
[38] Y. J. Chang, L. Moreschini, A. Bostwick, G. A. Gaines, Y. S. Kim, A. L. Walter, B. Freelon, A. Tebano, K. Horn, and E. Rotenberg, Phys. Rev. Lett. **111**, 126401 (2013).